Koivu, J., Myllyla, R., Helaakoski, T., Pihlajaniemi, T., Tasanen, K., & Kivirikko, K. I. (1987) *J. Biol. Chem. 262*, 6447-6449.
Laemmli, U. K. (1970) *Nature 227*, 680-685.
Lambert, N., & Freedman, R. B. (1983) *Biochem. J. 213*, 225-234.
Lowry, O. H., Rosebrough, N. J., Farr, A. L., & Randall, R. J. (1951) *J. Biol. Chem. 193*, 265-275.
McLean, L. R., & Hagaman, K. A. (1989) *Biochemistry 28*, 321-327.
Munro, S., & Pelham, H. R. B. (1987) *Cell 48*, 899-907.
Olsen, B. R., Berg, R. A., Kivirikko, K. I., & Prockop, D. J. (1973) *Eur. J. Biochem. 35*, 135-147.
Tuderman, L., Oikarinen, A., & Kivirikko, K. I. (1977) *Eur. J. Biochem. 78*, 547-556.
Vaux, D., Tooze, J., & Fuller, S. (1990) *Nature 345*, 495-502.
Wetterau, J. R., & Zilversmit, D. B. (1984) *J. Biol. Chem. 259*, 10863-10866.
Wetterau, J. R., & Zilversmit, D. B. (1985) *Chem. Phys. Lipids 38*, 205-222.
Wetterau, J. R., & Zilversmit, D. B. (1986) *Biochem. Biophys. Acta 875*, 610-617.
Wetterau, J. R., Combs, K. A., Spinner, S. N., & Joiner, B. J. (1990) *J. Biol. Chem. 265*, 9800-9807.
Wirtz, K. W. A. (1982) in *Lipid-Protein Interactions* (Griffith, O. H. & Jost, P. C., Eds.) Vol. 1, pp 151-231, John Wiley & Sons, Inc., New York.
Yang, Y. R., & Schachman, H. K. (1987) *Anal. Biochem. 163*, 188-195.
Yang, J. T., Wu, C. S. C., & Martinez, H. M. (1986) *Methods Enzymol. 130*, 208-269.
Yphantis, D. A. (1964) *Biochemistry 3*, 297-317.

Conformational Transition of Fructose-1,6-bisphosphatase: Structure Comparison between the AMP Complex (T form) and the Fructose 6-Phosphate Complex (R form)†

Hengming Ke,‡ Jiin-Yun Liang, Yiping Zhang, and William N. Lipscomb*
Gibbs Chemical Laboratory, Harvard University, 12 Oxford Street, Cambridge, Massachusetts 02138
Received November 30, 1990; Revised Manuscript Received February 14, 1991

ABSTRACT: A structure of the neutral form of fructose-1,6-bisphosphatase complexed with AMP has been determined by the molecular replacement method and refined at a 2.5-Å resolution to a crystallographic *R* factor of 0.169. The root-mean-square errors of the structure from standard geometry are 0.013 Å for bond lengths and 2.99° for bond angles. Comparison of the AMP complex with the F6P complex shows that dimer C3-C4 twists about 19° about a molecular 2-fold axis when dimers C1-C2 of the R and T forms of the enzyme are superimposed one another and that a slight shift of about 1 Å of the AMP domain partially compensates this twist. The R to T transition of the enzyme does not significantly change the conformation of the F6P-binding site. However, residues at the divalent metal site and the AMP site show significant positional shifts. If these results can be extended to substrate in place of F6P, they suggest that regulation of the enzyme by AMP may occur partly through effects on metal-ion affinity or position. AMP binds to the same sites of the T and R forms, but only half-occupancy was observed in the alkaline R form. Sequential binding of AMP, at least in pairs, is suggested as the unligated R form is converted to the T form. Two possible pathways are suggested for allosteric communication over about 28 Å between the AMP site and the active site: one via helices H1, H2, and H3 and another via the eight-stranded β-sheet. In the former case, the loop of residues 54-68, which joins helices H2 and H3, may play an important role in the allosteric inhibition, compatible with the kinetic observation that the AMP inhibition is decreased or completely lost by proteolytic cleavages in the loop. Careful inspection of the interchain interfaces reveals that a few residues at the interface between dimers may be critical to lock the enzyme in either a T or R form.

Fructose-1,6-bisphosphatase (D-fructose 1,6-bisphosphate 1-phosphohydrolase, EC 3.1.3.11, abbreviated as Fru-1,6-Pase),[1] a key regulatory enzyme in gluconeogenesis, catalyzes the hydrolysis of fructose 1,6-bisphosphate (Fru-1,6-P_2) to fructose 6-phosphate (F6P) and inorganic phosphate (Benkovic & deMaine, 1982; Tejwani, 1983). Fru-1,6-Pase isolated from various sources consists of four identical polypeptide chains that aggregate into a relatively flat tetramer (Figure 1). The activity of Fru-1,6-Pase is regulated in vivo by an allosteric inhibitor AMP and also by a substrate analogue fructose 2,6-bisphosphate (Fru-2,6-P_2). Binding of Fru-2,6-P_2 was contradictorily suggested at the active site (Pilkis et al., 1987), at an allosteric site (Van Schaftingen, 1987), or at both (Meek & Nimmo, 1983). Details of the three-dimensional structures of the unligated Fru-1,6-Pase and its complex with Fru-2,6-P_2 have located the 6-phosphate and furanose of Fru-2,6-P_2 at

†Supported by the National Institutes of Health Grant GM06920.
‡Present address: Department of Biochemistry and Biophysics, School of Medicine, The University of North Carolina, Chapel Hill, NC 27599.

[1] Abbreviations: Fru-1,6-Pase, fructose-1,6-bisphosphatase; Fru-2,6-P_2, fructose 2,6-bisphosphate; F6P, fructose 6-phosphate.

0006-2960/91/0430-4412$02.50/0 © 1991 American Chemical Society

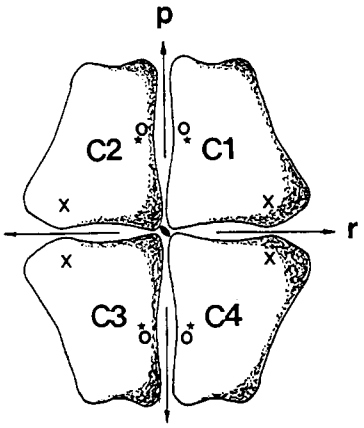

FIGURE 1: Schematic diagram of fructose-1,6-bisphosphatase looking down a molecular 2-fold axis q (labeled as the tilted oval dot in the center of picture). The other two molecular 2-fold axes are labeled as p (vertical) and r (horizontal). The molecule has $D2$ symmetry. The whole tetramer makes up the crystallographic asymmetric unit in the space group $P2_12_12_1$. The molecular 2-fold axis perpendicular to the paper plane is almost parallel to the crystallographic b axis. The molecular 2-fold axis p is about 13.5° off the crystallographic c axis. The F6P binding site is marked as "O", the divalent metal site as ★, and the AMP site as "X". The metal and F6P sites form the active site of the enzyme. The closest distance between the AMP and F6P sites is about 28 Å, while the AMP site in the C1 chain is about 16 Å from the AMP site in the C4 chain.

the active site of the enzyme, but the 2-phosphate is either disordered or possibly hydrolyzed (Ke et al., 1990a).

Potential multiple conformational states of Fru-1,6-Pase were implied by kinetic observations (Kemp & Marcus, 1990; Scheffler & Fromm, 1986) such as the synergistic inhibition by AMP in the presence of Fru-2,6-P_2 or vice versa (Van Schaftingen & Hers, 1981; Pilkis et al., 1981). Direct evidence comes from the structure of the F6P–AMP–Mg complex (Ke et al., 1990b), which has a different quaternary structure from that of the unligated enzyme. Also, we have established that the structure of the neutral form of Fru-1,6-Pase complexed with AMP has the same quaternary structure as the F6P–AMP–Mg complex. Thus, these two AMP complexes are identified as the T state of the enzyme. On the other hand, the F6P or Fru-2,6-P_2 complex as well as the unligated enzyme exist in the R state of the enzyme or in a close approximation to the R state.

We present in this paper the structural determination of the AMP complex and a detailed comparison between the AMP complex and the F6P complex. The structure of the F6P complex has been refined at a 2.1-Å resolution and will be reported elsewhere (Ke et al., 1991). The atomic coordinates of both the AMP complex and the F6P complex have been deposited with the Brookhaven Protein Data Bank as 4FBP and 5FBP.

Experimental Procedures and Results

The pig kidney Fru-1,6-Pase is a tetrameric molecule with four identical subunits, each of which has 335 amino acids and a molecular mass of 36 534 Da calculated from the amino acid sequence (Marcus et al., 1982). The neutral form of Fru-1,6-Pase was purified from pig kidney (Ke et al., 1990a) and cocrystallized with 1 mM AMP by dialyzing a 10–15 mg/mL protein solution against a buffer containing 20 mM tris(hydroxymethyl)aminomethane (Tris), 0.1 mM EDTA, 5 mM NaN_3, 1 mM β-mercaptoethanol, and 12% (w/v) polyethyleneglycol (molecular mass 3350 daltons) at pH 7.4. A four- to seven-day dialysis yielded crystals with two different morphologies of either rectangular bars or irregular hexahedrons. The latter had the space group $P1$ and diffracted poorly. Rectangular crystals with a typical size of 0.4 × 0.5 × 1.5 mm had the space group $P2_12_12_1$ with unit-cell dimensions of a = 78.5, b = 88.5, and c = 211.1 Å and showed diffraction to better than 2.0-Å resolution in X-ray photographs of stationary crystals. One tetramer is present in the crystallographic asymmetric unit of this unit cell.

The diffraction data were collected on the Mark III system of a multiwire X-ray area detector in the laboratory of Dr. Nguyen huu Xuong at University of California, San Diego. A total of 179 560 measured diffraction maxima were reduced to 47 359 unique reflections with an R_{sym} of 6.4%. These data are nearly complete to a 2.5-Å resolution and also include 856 reflections at higher resolution.

The recently refined structure of the F6P–AMP–Mg complex (Ke et al., 1990b) in the space group $P2_12_12$ was used as an initial model for the molecular replacement method. The C1–C2 dimer of the F6P–AMP–Mg structure (Figure 1) was placed in a large artificial $P1$ cell in order to obtain structure factors. Crowther's cross-rotation function (Crowther, 1972) was then calculated for several resolution shells with different intensity cut-off values. These calculations for different shells consistently showed the two strongest peaks at $\alpha = 2.5°$, $\beta = 78°$, and $\gamma = -90°$ and $\alpha = 177.5°$, $\beta = 102°$, and $\gamma = 90°$. These two solutions indicated an orientation of a molecular 2-fold axis that is almost coincident with the crystallographic Y axis (the axis perpendicular to the paper in Figure 1). Calculation of the cross-rotation function using the tetramer instead of a dimer as the initial model gave a similar result. A dimer generated from the first solution of the rotation function was placed in the real cell of $P2_12_12_1$, and the R factor search was carried out by use of the translation function (Machin, 1985) for shells at a resolution from 10 to 5 Å. This correctly positioned dimer yielded the lowest R factor of 0.375 for 1069 reflections within a 10- to 5-Å resolution. The second dimer was generated by a 180° rotation of the first dimer about the Y axis, and a similar translation search yielded the lowest R factor of 0.429. Examination of contacts between dimers in the graphics system PS390 confirmed the correctness of the search.

Taken as two rigid bodies, one for each dimer, the model from the molecular replacement was refined by 100 cycles of energy minimization of XPLOR (Brünger et al., 1987) against the 4012 reflections between a 10- and 5.5-Å resolution; the R factor dropped from 0.542 to 0.339. Although very small changes of the rotational angles and the translations occurred for the dimer C1–C2, a change of up to 9° in rotational angle and a shift of more than 3 Å of the translations occurred for the dimer C3–C4. The second step of the rigid-body refinement was carried out by taking each monomer as a rigid body. Here, the R factor further dropped to 0.291 for 44 260 reflections between a 10.0- and 2.5-Å resolution. This step of refinement did not substantially change the orientations of the four monomers.

The structure from the rigid-body refinement was then rebuilt by using the program FRODO (Jones, 1982). Several cycles of energy minimization by XPLOR and manual rebuilding brought the R factor to 0.208 without adding solvent molecules. Solvent molecules were automatically picked up by searching strong peaks in the $F_o - F_c$ map and by checking for satisfactory interactions with protein residues before their coordinates were retained for further refinement. The coordinates of those solvent molecules that have high temperature factors (>50 Å^2) after further refinement were deleted. Solvent searching and refinement were repeated until no peaks that had electron density three times stronger than the

background were found in the $F_o - F_c$ map.

The final AMP structure that includes 383 water molecules associated with the tetramer has a crystallographic R factor of 0.169 for 42 390 reflections at a 10- to 2.5-Å resolution. The root-mean-square errors are 0.013 Å and 2.99° from the ideal geometry of bond lengths and bond angles, respectively. The overall average B factor for all residues of the tetramer is 21.5 Å^2. However, the average B factor of 16.7 Å^2 for all atoms of the dimer C1–C2 is obviously lower than that of 26.3 Å^2 for the dimer C3–C4. As shown in Figure 2, the distribution of the average B values for backbone atoms against residue number is similar among the four subunits. A similar distribution occurs for the side-chain atoms. In more detail, the loops around residues 269 and 127 have high B values in all four chains, indicating a disordered pattern of those residues. The loop around 235 has high B values in the C3–C4 dimer but low B values in the C1–C2 dimer. The B values are high for the loop of residues 142–155 in the C1, C3, and C4 chains but comparable with the overall average B factor in the C2 chain. Generally, a higher B value indicates a more flexible fragment. Although intermolecular contacts may influence these flexible regions, reasonably consistently high B values among the different chains are evidence for the intrinsic disorder of the region in the isolated molecule.

The electron-density maps with either $2F_o - F_c$ or $F_o - F_c$ as coefficients clearly showed complete traces of residues 54–61 in four monomers except for partial disorder in one of the four chains (C1). These residues had not been visible in the maps of the unligated enzyme (Ke et al., 1989). Residues before 9 had no reasonable density in the present AMP complex. Corresponding to high B values, electron density for the loops of residues 123–128, 142–155, 233–237, and 268–272 in the tetramer are poor, except that 142–155 in C2 and 233–237 in C1 and C2 are comparatively well ordered.

Discussion

The R to T Transition of Fru-1,6-Pase. We have reported that the enzyme complex with AMP, F6P, and Mg^{2+} exists in a T conformational state of the enzyme (Ke et al., 1990b). The present study shows that the AMP complex also exists in a T state of the enzyme. Superposition of the two T forms shows that the secondary and quaternary structures are the same. On other hand, the structures of the unligated Fru-1,6-Pase and its complexes with the product F6P in the presence or absence of magnesium (Ke, Zhang, Liang, and Lipscomb, unpublished results) or with the competitive inhibitor Fru-2,6-P_2, which may have hydrolyzed to F6P (Ke et al., 1990a), or with substrate Fru-1,6-P_2 in the absence of a divalent metal ion (Ke, Zhang, and Lipscomb, unpublished results) have the R conformational state of the enzyme or very nearly so. Of these structures, the unligated enzyme shows 1–2% changes along each cell dimension in comparison to the F6P or Fru-1,6-P_2 complex. Our crystallographic study shows that AMP itself can lock Fru-1,6-Pase into a T state. It is interesting to note that the opposing enzyme 1-phosphofructokinase has the R form for the unligated enzyme (in the crystal) and is structurally locked in the T conformation by the allosteric inhibitor phosphoenolpyruvate (Schirmer & Evans, 1990).

When the full tetramer of the F6P structure is superimposed over the AMP structure by the computer program XPLOR (Brünger et al., 1987) or SUPERIMP (Honzatko, 1986), two major quaternary conformational changes are observed: (1) a twist of the dimer C3–C4 about the molecular 2-fold axis p by about 19° relative to the dimer C1–C2 (Figures 1 and 3), and (2) a translation of about 1 Å of the AMP domains

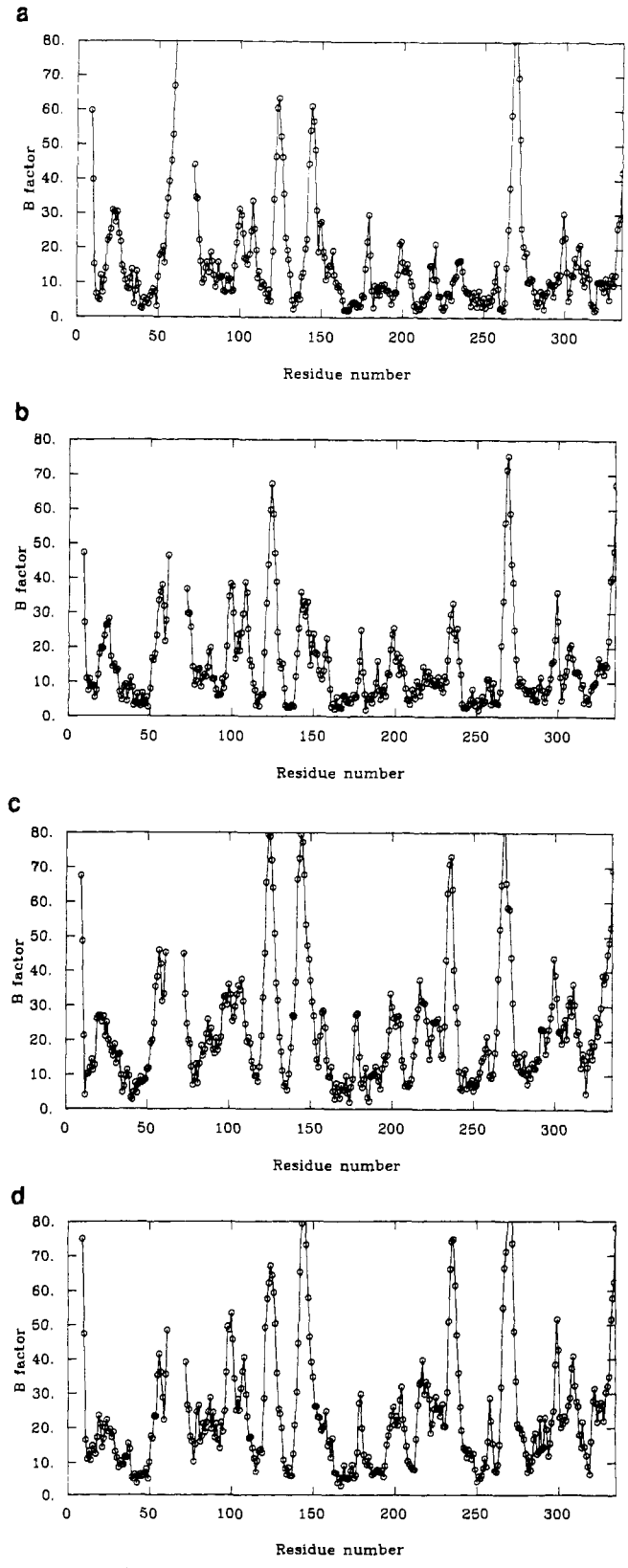

FIGURE 2: Plot of the average B value for backbone atoms against residue for (a) the C1 chain, (b) the C2 chain, (c) the C3 chain, and (d) the C4 chain. Although the average B value for the dimer C1–C2 is smaller than those of the C3–C4, the distribution of B values along the chain is similar among the four chains.

of both dimers C1–C2 and C3–C4 (Figure 4). In addition, superposition of the dimer C1–C2 of the AMP complex over that of the F6P complex shows an average displacement of 0.71 Å for all Cα atoms: 0.99 Å for the AMP domain (residues 9–200) and 0.35 Å for the FBP domain (residues

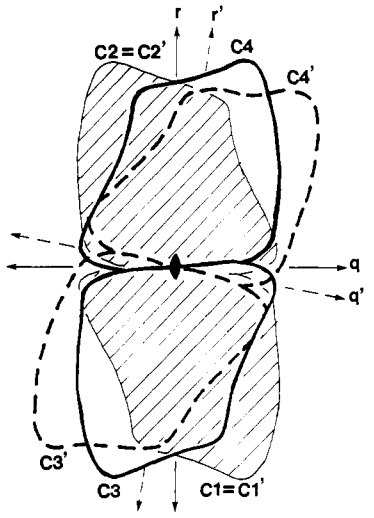

FIGURE 3: Schematic drawing of the superposition of the F6P complex on the AMP complex viewed along the molecular 2-fold axis p in Figure 1. Dimers C1–C2 of the T and R forms are superimposed and drawn as shaded regions. The heavy solid lines represent dimer C3–C4 of the F6P complex while the broken lines are those of the AMP complex. Dimer C3′–C4′ of the AMP complex is twisted about 19° about the molecular 2-fold axis p relative to the same dimer of the F6P complex when the F6P complex is transformed to the AMP complex. Correspondingly, molecular 2-fold axes q and r rotate about 9.5° from the initial position (solid line) to the broken-line position.

Table I: Interactions between AMP and Fru-1,6-Pase

atom of AMP[a]	residue and atom of protein[a]	contact type[b]
phosphate group		
OR	Glu29, N; Met30, N	H
OL	Thr27, N; Thr27, OG1	H
O′	Lys112, NZ; Tyr113, OH	H
ribose ring		
O2′	Val160, CG1	V
O3′	Tyr113, OH; Arg140, NH1	H
O5′	Tyr113, NH	H
adenine base		
N9	Ala24, CB	V
C8	Met30, CB; Gly26, CA	V
N7	Met30, CB; Gly21, CA	V
	Thr31, OG1	V
C5	Gly21, CA	V
C4	Ala24, CA	V
N3	Ala24, CB	V
C2	Met177, SD	V
N1	Met177, SD	V
N6	Val17, O; Thr31, OG1	H

[a] Atom names are defined in the same way as in program FRODO. [b] H represents a hydrogen bond or salt link within a 2.5–3.2-Å radius. V represents a van der Waals contact or polar interaction within a 3.2–3.8-Å radius.

201–335). Large movement of residues in the AMP domain is visible when the displacement of Cα atoms between T and R forms, which is calculated by the computer program SUPERIMP (Honzatko, 1986), is plotted against each residue (Figure 5). Of course, the large displacements of residues 234–237 and 268–272 in Figure 5 are less reliable because of partial disorder of these loops in both the T and R forms. Exhibition of the resultant superposition of the T and R forms using the graphics system PS390 clearly shows consistent shifts of residues in the AMP domain, amounting to an overall movement of about 1 Å for the AMP domain.

Changes at the AMP-Binding Site. The four binding sites of AMP per tetramer (one site per monomer) show equally strong electron density in the $2F_o - F_c$ or $F_o - F_c$ maps that were calculated by omitting AMP. No density for AMP was evident at the active sites of the enzyme. Here, the AMP complex was cocrystallized with the neutral form of the enzyme from a solution of 1 mM AMP. The binding site of AMP occurs between the helix layer (H1, H2, H3, residues 9–90, at the bottom layer in Figure 4) and the eight-stranded β-sheet (B1–B8, residues 90–200). This is the same site as we previously observed in the T form of the AMP–F6P–Mg complex (Ke et al., 1990b) and in the R form of the AMP complex with the alkaline form of the enzyme in the space group $P3_221$ (Ke et al., 1989).

As listed in Table I, the phosphate group of AMP interacts with the backbone atoms of Glu29 and Met30 and the side-chain atoms of Thr27, Lys112, and Tyr113 in all four crystallographically independent chains of the tetramer. The adenine base of AMP is located in a hydrophobic environment, involving residues from helices H1 (12–24) and H2 (28–50) and β-turn T3 (177–180). Detailed comparison of the AMP complex with the F6P complex shows significant changes in the AMP-binding site (Figure 6). The largest shifts of Cα atoms at the AMP site are about 1.3 Å for α-helix H1 and about 1.2 Å for α-helix H2. In addition, residues near AMP such as Arg140, Val160, and Met177 show Cα shifts of about 0.5 Å between the T and R forms (Figure 5).

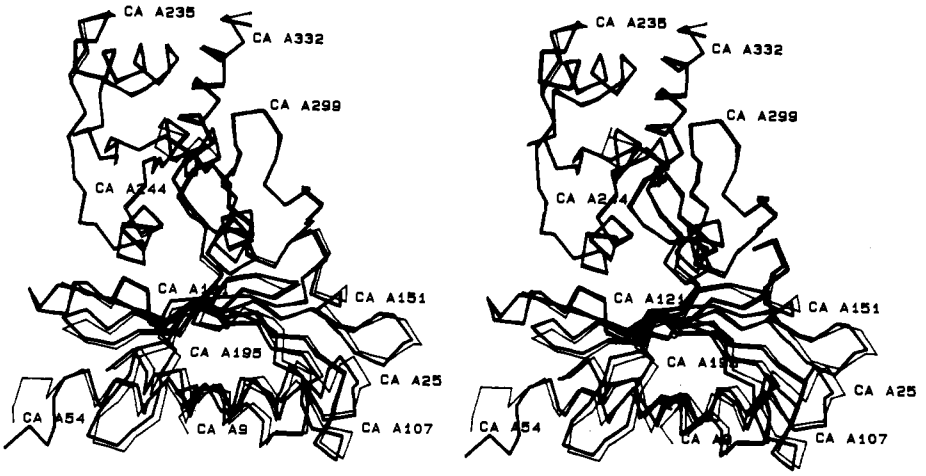

FIGURE 4: Stereo drawing of superposition of Cα atoms of the F6P complex over the AMP complex, viewing in the same way as in Figure 1. The thicker lines represent the F6P complex, while the thinner lines are the AMP complex. The FBP domains (the upper part of the figure, residues after 201) are completely superimposible, while the AMP domains have an averaged shift of 1 Å. Ala51 and Gly52 in the AMP complex can be placed in two possible traces, one of which is the same as is observed in the F6P complex. The traces of Ala51 and Gly52 shown in the drawing are different for the T and R forms.

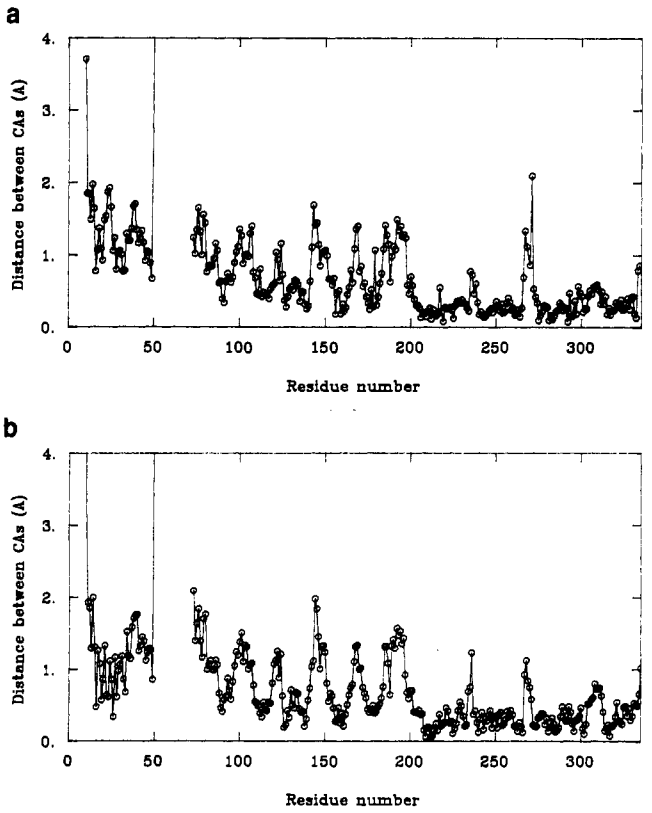

FIGURE 5: Plot of Cα atom displacement against each residue for the superposition of (a) the C1 chain and (b) the C2 chain by SUPERIMP (Honzatko, 1986). The average displacement of Cα atoms is 0.99 Å for residues 9–200 in comparison to 0.35 Å for residues 201–335. Large displacements around residues 235 and 269 are less reliable because of disorder of these two loops in both the *T* and *R* forms.

In a previous study (Ke et al., 1989), crystals of the alkaline form of the enzyme grown in the presence of 1 mM AMP showed that AMP was bound at half-occupancy in the C1 (and C4) but not in the C2 (and C3) chains. The enzyme of that study showed partial proteolysis, and the crystals diffracted relatively poorly. This crystal structure in the space group $P3_221$ showed an intermolecular interaction between Asn142 and AMP (Ke et al., 1989). Recent refinement of the F6P complex at a 2.1-Å resolution with the neutral form of the enzyme that has little or no proteolytic cleavage has shown that AMP-binding residues 20–27 are ordered in the C1 chain but disordered in the C2 chain, and thus AMP would be expected to bind in C1 in preference to C2 in these crystals

Table II: Interactions of F6P with the Active-Site Residues

atom of F6P	distance to C1 (Å)[a]	distance to C2 (Å)[a]
phosphate group		
O21	2.69; OH, Tyr244	2.85; OH, Tyr 244
O21	2.82; ND2, Asn212	2.85; ND2, Asn212
O21	3.20; NH2, Arg243	
O22	2.65; NH1, Arg243	2.69; NH1, Arg243
O22	2.72; O, Wat503	2.58; O, Wat359
O22	3.06; O, Wat500	2.89; O, Wat361
O23	2.69; OH, Tyr215	2.82; OH, Tyr215
O23	2.81; OH, Tyr264	2.74; OH, Tyr264
O23	2.59; O, Wat502	3.07; O, Wat357
furanose ring		
O6	3.19; NZ, Lys274	2.87; NZ, Lys274
O5	2.82; NZ, Lys274	2.64; NZ, Lys274
O4	2.57; O, Wat505	2.71; O, Wat356
O3	2.74, N, Met248	2.73, N, Met248
O3	2.89, OD2, Asp121	3.20; OD2, Asp121
O3	2.68; O, Wat504	3.13; OD1, Asp121
O2		2.79; O, Wat358
O1	3.06; OE1, Glu280	
O1	2.93; O, Wat501	

[a] Atom names are defined as in program FRODO. Reside Arg243 comes from the neighboring chain.

($P3_221$). While it is possible that intrinsic molecular asymmetry is present in the R form of a molecule in solution, this asymmetry may be caused by intermolecular interactions in this crystalline form or may occur at less than full occupancy of ligands as an effect of local negative cooperativity in reducing the symmetry of the oligomeric molecule.

Kinetic experiments have reported either two or four sites of Fru-1,6-Pase for AMP binding (Nimmo & Tipton, 1975; Tejwani et al., 1976; Pontremoli et al., 1968; Kratowich & Mendicino, 1974; Marcus & Haley, 1979; McGrane et al., 1983). The different results may reflect the various degrees of hydrolysis of the enzyme during purification. The binding of AMP is decreased or even abolished due to the proteolytic cleavage. If proteolysis inhibits the R to T transition and if the asymmetry is intrinsic to the molecule in solution or is developed by subsaturated AMP binding, this binding of AMP may be partially sequential: (1) AMP binds to the C1 (C4) chain in the R form, (2) the enzyme converts to (or toward) the T form, and (3) AMP binds to the C2 (C3) chain to lock the enzyme into the T form.

Changes at the Active Site. In the recently refined F6P structure (Ke et al., 1991), the 6-phosphate of F6P interacts with Asn212, Tyr215, Tyr244, and Tyr264 of the same monomer and Arg243 of the neighboring monomer. The furanose

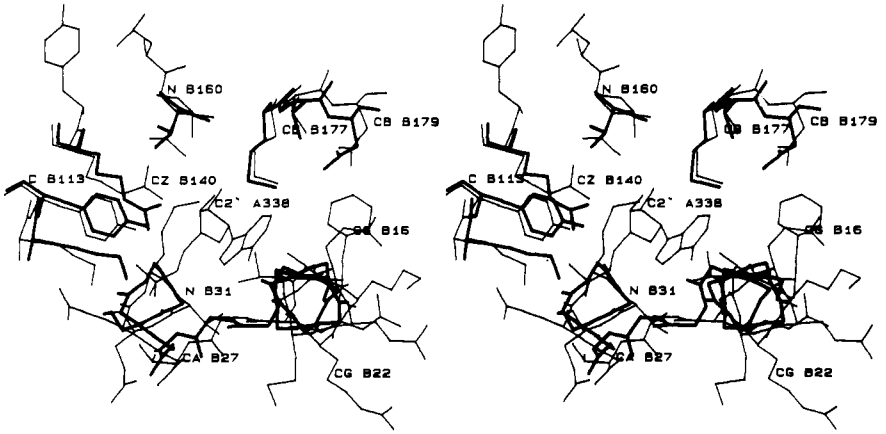

FIGURE 6: Stereoplot of the AMP-binding site from the superposition of the R and T forms. The thinner lines represent the residues from the AMP complex, while the thicker lines are from the F6P complex. Helices H1 (right corner) and H2 (middle bottom) are visible. AMP is labeled as A338 in the center of the picture and its detailed interactions with the enzyme are listed in Table I. The residues of H1 and H2 of the F6P complex are represented by Cα atoms only.

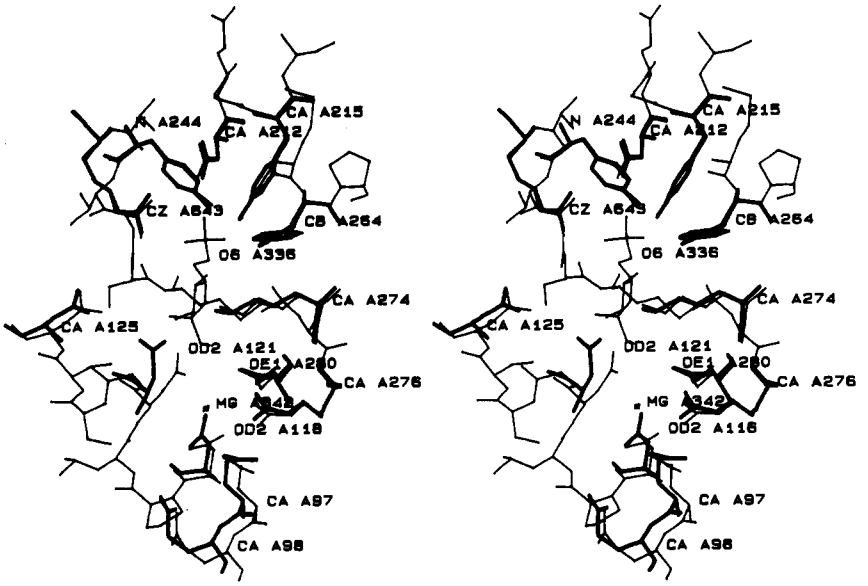

FIGURE 7: Stereoplot of the F6P-binding site from the superposition of the R and T forms. The thinner lines represent the residues from the F6P complex, while the thicker lines represent those from the AMP complex. The Mg^{2+} ion is labeled as "MG A342". F6P is labeled as A336 in the middle of the drawing. The F6P-binding residues Arg243 (labeled as A643), Tyr244, Asn212, Tyr215, Tyr264, and Lys274 (at the top of the figure, from left to right, clockwise) superimpose perfectly. However, the residues at the divalent metal site, such as Glu97, Glu98, Asp118, and Asp121, show shifts of over 1 Å in Cα positions.

ring of F6P binds mainly to Lys274 (Table II, Figure 7). These interactions also occur in the structure of the F6P–AMP–Mg complex (Ke et al., 1990b). Superposition of the F6P complex over the AMP complex shows only small changes at the F6P-binding site (Figure 7). For example, Cα positions of those residues interacting with the 6-phosphate group differ by only about 0.2 Å, in comparison to the average of 0.35 Å for all Cα atoms of the FBP domain in these two complexes. However, the divalent metal binding site, a portion of the active site known as the negatively charged pocket (Ke et al., 1989, 1990a), shows somewhat larger changes. The Cα positions of residues Glu97, Glu98, and Asp121 shift over 1 Å, while Cα positions for other divalent metal binding residues Asp118 and Glu280 move 0.5 and 0.3 Å, respectively.

The kinetic observations, that AMP does not affect the stoichiometry of Fru-2,6-P_2 binding or the associated negative cooperativity (McGrane et al., 1983) and that the binding of the substrate and its analogue α- and β-methyl-D-fructofuranoside 1,6-bisphosphate is not affected by AMP (Sarngadharan et al., 1969; Benkovic et al., 1978) are consistent with lack of significant changes in the conformation of the F6P-binding site. We assume here that the 6-phosphate group of the substrate analogues has essentially the same binding as the 6-phosphate of F6P. On the other hand, the inhibition by AMP and Fru-2,6-P_2 is synergistic (Van Schaftingen & Hers, 1981; Pilkis et al., 1981): the K_i for Fru-2,6-P_2 decreases from 5.3 to 1.2 μM in the presence of 5 μM AMP (Pontremoli et al., 1982). We suggest that further structure studies will provide a basis for this synergistic inhibition.

Our findings that AMP binding changes the conformation of the metal site, but not the F6P site, are consistent with the kinetic observations that AMP in the presence of substrate causes a decrease in the apparent binding constants for Mg^{2+} or Mn^{2+} ions (Nimmo & Tipton, 1975; Liu & Fromm, 1990), that Mg^{2+} decreases both the binding and the inhibition of AMP (Pontremoli et al., 1968; Nimmo & Tipton (1975); Sarngadharan et al., 1969), and that the inhibition of turkey liver Fru-1,6-Pase by Zn^{2+} and AMP is synergistic (Han et al., 1980). Further structure studies of AMP complexes in the presence of metal ions and α-fructose 1,6-bisphosphate or its analogues are needed.

Changes of the Interfacial Interactions. The tetrameric Fru-1,6-Pase has two major kinds of interfacial interactions, the interdimeric interface (C1–C4 and C2–C3 interfaces in Figure 1) and intradimeric interface (C1–C2 and C3–C4 interfaces). In addition, a few interactions between C1–C3 or C2–C4 are found in the AMP complex, but not in the F6P complex.

The interdimeric interface is mainly made up of helices H1, H2, and H3. In the R form of the F6P complex, the upper H1 (C1 or C2) is close to the lower H3 (C4 or C3), the upper H2 to the lower H2, and the upper H3 to the lower H1 (Figure 8a). The largest changes in the R to T transition occur in this interface. The 19° twist of the dimer C3–C4, when the enzyme changes its conformation from R to T, places the upper H2 close to the lower H3 in the T form of the AMP complex and conversely (Figure 8b). Although many interactions are conserved in this large rearrangement, others disappear and some new interactions are formed (Table III). Some residues appear to lock the enzyme in either the T or the R state. For example, Arg22 in the C1 chain forms a hydrogen bond with the backbone oxygen of Thr27 of the C4 chain in the AMP complex but contacts backbone atoms of Glu108 and Arg110 in the F6P complex (Table III, Figure 8a,b). Arg22 is a residue of H1, an α-helix that binds AMP (Figure 6). This arginine interacts with Thr27, which bonds to AMP in the AMP complex. Thus Arg22 is probably a good candidate for a key residue in the conformational transition. Moreover, Arg22 is conserved in the mammalian and yeast enzymes that are inhibited by AMP, but mutated to methionine or glutamine in chloroplast enzymes that are not inhibited by AMP (Raines et al., 1988; Marcus & Harrsch, 1990, and references therein). In addition, residue Asn9 in the C1 chain, which switches its interactions from Ser87 in the T form to Asn83 in the R form (Table III), may be another candidate for a key residue in the R to T transition. Site-specific mutagenic experiments are suggested for these residues, as well as for those in the active and the regulatory sites.

The C1–C2 (or equivalent C3–C4) interface composed of the FBP–FBP domains (residues 201–335) and the AMP–AMP domains (residues 1–200). There are no substantial changes of the FBP–FBP domain interactions (Table III),

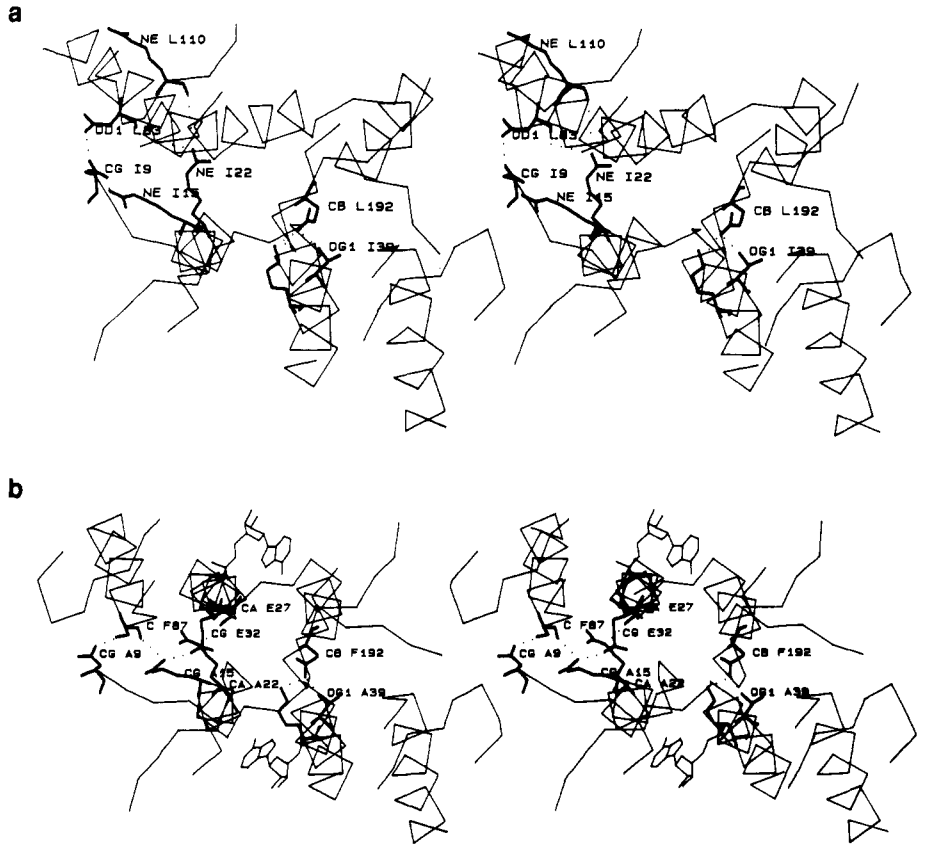

FIGURE 8: Stereo drawing of the C1–C4 interfacial domain, viewed along the molecular axis *r* in Figure 1. The molecular skeletons are drawn for Cα atoms by using thin lines, including residues 9–50, 72–90, 105–113, and 185–197 of the C1 and C4 chains. Helices H1 (Thr12–Ala24), H2 (Gly28–Lys50) and H3 (Lys72–Ser88) are arranged from left to right near the bottom for the C1 chain and from right to left near the top for the C4 chain. Some important residues in or near the interface are drawn in thick lines, and their hydrogen-bond scheme is shown by dotted lines. Figure 8a is the C1–C4 interface domain of the F6P complex, while Figure 8b is that of the AMP complex. AMP-binding sites are shown at the top center and bottom center of Figure 8b. In this interface of the F6P complex, H1 of the C1 chain is spatially close to H3 of the C4 chain and conversely. In contrast, H1 is closer to H2, and conversely, in the AMP complex.

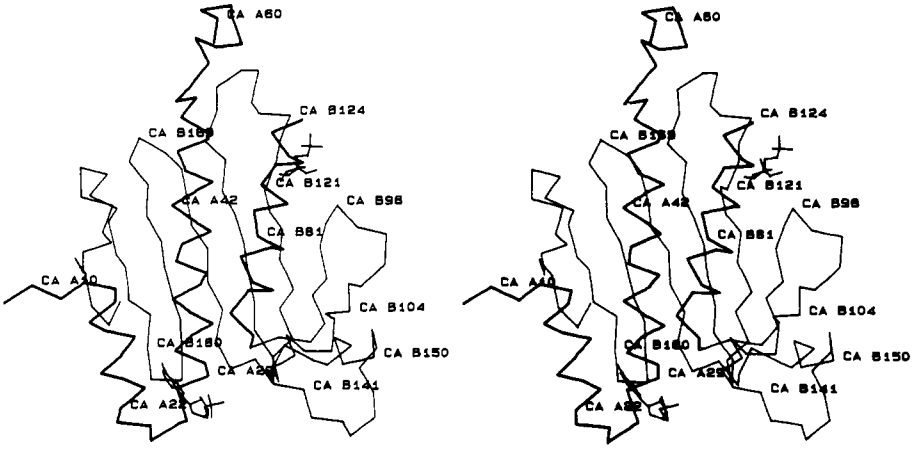

FIGURE 9: Stereo presentation of possible communication between the AMP site and the active site. Only Cα atoms are shown for residues 9–61 and 72–200 of the C1 chain. AMP drawn at the bottom binds between the helix layer (H1, H2, and H3, from left to right, represented by thicker lines) and the eight-stranded β-sheet (thinner lines). F6P drawn at the top right marks the active site of the enzyme.

consistent with insignificant shifts of Cα atoms of the FBP domain (Figure 5) when the enzyme converts from the R to T state. In the AMP–AMP domain, interaction changes are observed for the loops of 166–170 and 50–53 (Table III). The electron density shows two possible traces for Ala51 to Gly52 for both the AMP complex and the F6P–AMP–Mg complex in the T forms, while in the R form of the F6P complex only one of these traces is observed. The interactions for Ala51 and Gly52 in Table III include both possible traces.

Potential Pathways of the Allosteric Inhibition. The distance of 28 Å from the AMP-binding site to the active site of the enzyme requires a mechanism of allosteric communication. AMP interacts with the residues of α-helices H1 and H2 and of the eight-stranded β-sheet (Figure 9). At least two pathways can be considered for the allosteric inhibition by AMP. One pathway involves the eight-stranded β-sheet. The AMP binding residues Lys112 and Tyr113 of β-strand B3 may be close enough to Asp118 and Asp121, which is located at another end of the B3 strand, to influence their conformations at the metal-binding site. Moreover, it is

Table III: Interchain Interactions of the T and R Fru-1,6-Pase

residue, atom[a]	residue, atom[a]	contact type[b]	complex
C1–C2 and C3–C4			
Asn9, O, C	Tyr57, O	H (C4–C3)	AMP
Asn9, N	Gly58, O	H (C4–C3)	AMP
Ile10, CG1, CG2, CB	Tyr57, O, CB	V	AMP
Ile10, CD1	Ile59, CD1, CB	V	AMP
Val148, CG1	Ser169, O	V	both
Arg49, NH2	Arg49, NH1	V	both
Arg49, NH2	Gly168, O	H	AMP
Arg49, NH2	Gly168, O	V(C2–C1)	F6P
Arg49, NH2, NE, CD, CG	Ser169, O, CA	H, V	AMP
Arg49, N, CA, CB, CG	Ser169, O	V	F6P
Arg49, O	Ala170, CB	V	F6P
Arg49, O	Pro188, CD, CG	V	AMP
Lys50, CG	Ala170, CB	V (C2–C1)	AMP
Lys50, NZ	Asp187, OD1, OD2	H (C2–C1)	F6P
Lys50, O	Pro188, CD	V	both
Ala51, O	Met185, SD, CE	V (C1–C2)	F6P
Ala51, CA, C	Asp187, CD2	V	AMP
Gly52, N, CA	Met185, SD	V (C2–C1)	F6P
Gly52, N, C, CA	Asp187, OD1, OD2, CG	H, V	AMP
Gly52, O, C	Val196, CB, CG1	V	F6P
Ile53, CD1, CG1	Met185, CB, CG	V (C2–C1)	F6P
Ile53, CD1	Leu186, O, C	V	F6P
Ile53, N, CD1	Asp187, CA, N, CB	V	both
Ala54, N, CB	Asp187, OD1	H, V	AMP
Ala54, CB	Ile190, CD1	V	AMP
Tyr57, CB, CG	Ile194, CG2	V	AMP
Tyr57, OH, CZ	Val197, CG1	V (C1–C2)	AMP
Cys128, O	His253, CD2	V	both
Cys128, CA, CB, SG	Val257, CD2	V	F6P
Cys128, SG	Tyr258, CB	V	F6P
Leu129, CB, CG, CD1	Leu166, CD2	V (C1–C2)	F6P
Leu129, O	Gly168, CA, C	V	AMP
Leu129, O, C	Ser169, N, OG	H, V	AMP
Leu129, CD1	Ala170, O, C	V (C1–C2)	F6P
Leu129, CD1	Met172, CB	V	AMP
Val130, O	Ser169, OG, CB	V	AMP
Ser131, OG	Ser131, OG	V	F6P
Tyr167, O	Ser169, CB	V	F6P
Gly168, O	Gly168, O	H	both
Gly168, O, C	Ser169, N, CA	V	F6P
Tyr209, OH	Glu213, O, C, CB	V	F6P
Tyr209, OH	Gly214, N	V	F6P
Asn212, OD1, CG, ND2	Ala242, N, O, CB, CA	H, V	both
Asn212, ND2	Arg243, NH2	V	both
Glu213, OE1, OE2, CD	Glu213, OE1, OE2, CD	V	both
Glu213, OE1, CD	Lys231, NZ, CD, CE	H, V	both
Gly214, O	Pro239, CB, CG	V	both
Gly214, O, CA, C	Tyr240, O	V	both
Gly214, N	Ala242, CB	V	both
Ala216, CB	Lys231, CD	V	both
Lys217, CA, CB	Lys231, O	V	F6P
Lys217, CA, CB	Phe232, CE1	V	both
Lys217, NZ	Ser237, O	H (C3–C4)	AMP
Ala242, O	Tyr244, CD2	V	both
Arg243, NH2, C, CA	Tyr244, O, CE2	V	both
Arg243, CD, NE	Val245, O	V	both
Arg243, NE	Gly246, CA	V	both
Tyr244, O, N, C, CA	Tyr244, N, O, C, CA	H, V	both
C1–C4 and C2–C3			
Phe6, CD1, CE1	Ala47, CB	V (C2–C3)	F6P
Phe6, Ca, O	Leu76, CD1	V	F6P
Phe6, CZ, CE2	Leu80, CD2	V (C2–C3)	F6P
Thr8, CG2	Leu76, O	V	F6P
Thr8, CB, CG2	Asp79, CB	V	F6P
Thr8, O	Leu80, CA, CD1	V (C2–C3)	F6P
Thr8, O	Asn83, CG, ND2, CB	N, V	F6P
Asn9, ND2	Asn83, OD1	H, V	F6P
Asn9, ND2, CB, CG, CA	Ser87, OG, CA, CB	H, V (C1–C4)	AMP
Asn9, ND2	Phe89, CE1, CZ	V (C1–C4)	AMP
Asn9, ND2, OD1	Lys109, CD, CE	V (C1–C4)	AMP
Ile10, CD1	Leu80, CD1	V (C2–C3)	F6P
Thr14, CG2	Asn35, CG, ND2	V	both
Arg15, NH2, O	Gln32, OE1	H (C1–C4)	AMP
Arg15, O, CG, CA	Gln32, OE1, NE2	V	AMP
Arg15, NH2, CD, NE	Ser87, O, OG	V (C1–C4)	both
Arg15, NH2	Ser87, O	H (C2–C3)	AMP
Arg15, NH2	Ser88, O	V (C1–C4)	AMP
Arg15, NH1, CZ	Phe89, CE1, CD1	V	AMP
Met18, SD	Met18, SD	V	AMP
Met18, CB, CG	Gln32, NE2, CD, OE1	V	both
Met18, CE	Ser87, O	V (C1–C4)	F6P
Met18, CE, C, O, SD	Phe89, CD1, CE1	V (C2–C3)	F6P
Glu19, CD, OE2	Gln32, OE1	V (C1–C4)	AMP
Glu19, OE2	Ser87, OG	V (C2–C3)	F6P
Glu19, OE2	Phe89, CE1, CZ	V	F6P
Arg22, NE, NH1	Thr27, O	H	AMP
Arg22, NH1	Glu29, N, CA, CB	V (C1–C4)	AMP
Arg22, CD, NE, CZ	Phe89, CB, CG, CE2	V	F6P
Arg22, NH1, NE, CZ	Glu108, O, C	H, V (C2–C3)	F6P
Arg22, NH1, NH2, CZ	Arg110, O, C, N	H, V (C2–C3)	F6P
Thr39, OG1, CG2	Glu192, OE2, CD	H, V	both
Lys42, NZ	Ile190, O	H	both
Lys42, NZ	Gly191, O	H	AMP
Lys42, NZ	Gly191, O	V	F6P
Lys42, NZ, CE	Glu192, OE2, CD	H, V	both
Ala43, CA	Ile190, CG2	V	both
Thr46, OG1	Ala189, O	H	both
Gly191, O	Gly191, O	V	AMP
C1–C3 and C2–C4			
Ile59, O, CG1	Leu80, CD2, CA	V	AMP
Ile59, O	Val84, CG2	V	AMP
Ala60, CG	Leu80, CD2	V	AMP
Ala60, CB	Asn83, ND2, CG	V	AMP

[a] Atom names are defined in the same way as in program FRODO. [b] H represents a hydrogen bond or salt link within a 2.5–3.2-Å radius while V represents a van der Waals contact or polar interaction within a 3.2–3.8-Å radius. The parentheses represent the contacts only existing between the chains.

possible that the whole eight-stranded sheet taken as a rigid body can be controlled and shifted by AMP binding to Tyr113 (at one end of B3), Arg140 (at one end of B4), Val160 (at one end of B5), and Met177 (the β-turn T3 linked to B6 and B7). Changes of this type could regulate metal and phosphate binding.

The second pathway may be via helices H1 and H2. Abundant interactions between AMP and H1 or residues at the top of H2 may propagate the allosteric information to the loop of 54–70 and thereby regulate the enzymatic reaction. Our metal-binding study showed that a minor zinc site bonds to Asp74 (Ke and Lipscomb, unpublished results). This binding geometry may imply that some residues in the loop 54–70 be spatially close to the metal-binding site. Also, kinetic experiments have shown that the hydrolysis of the enzyme by unknown proteases is accompanied by a decrease or loss of

the AMP inhibition (Marcus, 1981), and residues 54–67 are identified as the major region of the proteolytic cleavage (Marcus et al., 1982). Since the proteolytically cleaved enzyme from various sources is still able to turn over the substrate, the loop 54–70 may be involved in the regulation of activity by its conformational change in a way either influencing the pathway of the allosteric inhibition or directly disturbing the metal binding.

In the T forms of the AMP complex and F6P–AMP–Mg complex, we found reasonably good electron density for residues 55–61 in comparison to no density in the R form of the F6P complex. This result for the R form is therefore clearly due to a disordered loop but not to proteolytic cleavage because microsequencing of the F6P complex from dissolved crystals shows a maximal hydrolysis of only 10% of the enzyme between Asn236 and Ser237. This difference of the conformation of the loop 54–61 and also the loop 50–53 could form one structural aspect of the AMP inhibition. The role of the loop 54–70, disordered in the R structure, could be studied further by site-directed mutagenesis.

Conclusion. We proposed in this paper (1) a possible sequential aspect to binding of AMP to the enzyme and (2) two plausible pathways of the AMP allosteric inhibition within a monomer. However, further studies are required to elucidate the allosteric communication within or between the dimers. The possibility that a few critical residues control the R to T transition may be too optimistic, but the structures provide a substantial basis for further studies of the mechanism of the allosteric inhibition in this and other allosteric proteins [Lipscomb, W. N. (1991) *Chemtracts*: *Biochem. Mol. Biol. 2*, 1–15].

ACKNOWLEDGMENTS

We thank the Pittsburgh Supercomputing Center and the National Science Foundation for support of the computing facilities. We also thank Dr. N. h. Xuong for the use of the data collection resource for crystallography at the University of California, San Diego (Grant RR01644), and Dr. F. Marcus of Chiron Corporation for the microsequencing of the crystals.

REFERENCES

Benkovic, S. J., & deMaine, M. M. (1982) *Adv. Enzymol. Relat. Areas Mol. Biol. 53*, 45–82.

Benkovic, P. A., Frey, W. A., & Benkovic, S. J. (1978) *Arch. Biochem. Biophys. 191*, 719–726.

Brünger, A. T., Kuriyan, J., & Karplus, M. (1987) *Science 235*, 458–460.

Crowther, R. A. (1972) in *The Molecular Replacement Method* (Rossmann, M. G., Ed.) pp 173–178, Gordon and Breach, New York.

Han, P. F., Han, G. Y., McBay, H. C., & Johnson, J., Jr. (1980) *Biochem. Biophys. Res. Commun. 93*, 558–565.

Honzatko, R. B. (1986) *Acta Crystallogr. A42*, 172–178.

Jones, T. A. (1982) in *Computational Crystallography* (Sayer, D., Ed.) pp 303–317, Oxford, London.

Ke, H. M., Thorpe, C. M., Seaton, B. A., Marcus, E., & Lipscomb, W. N. (1989) *Proc. Natl. Acad. Sci. U.S.A. 86*, 1475–1479.

Ke, H. M., Thorpe, C. M., Seaton, B. A., Lipscomb, W. N., & Marcus, F. (1990a) *J. Mol. Biol. 212*, 513–539.

Ke, H. M., Zhang, Y. P., & Lipscomb, W. N. (1990b) *Proc. Natl. Acad. Sci. U.S.A. 87*, 5243–5247.

Ke, H. M., Zhang, Y. P., Liang, J. Y., & Lipscomb, W. N. (1991) *Proc. Natl. Acad. Sci. U.S.A. 88*, 2989–2993.

Kemp, R. G., & Marcus, F. (1990) in *Fructose-2,6-bisphosphate* (Pilkis, S. J., Ed.) pp 17–37, CRC Press, Florida.

Kratowich, N., & Mendicino, J. (1974) *J. Biol. Chem. 249*, 5485–5494.

Liu, F., & Fromm, H. J. (1990) *J. Biol. Chem. 265*, 7401–7406.

Machin, P. A. (1985) *Molecular Replacement*, Daresbury Laboratory.

Marcus, F. (1981) in *The Regulation of Carbohydrate Formation and Utilization in Mammals* (Veneziale. C. M., Ed.) pp 269–290, University Park Press, Baltimore, MD.

Marcus, F., & Haley, B. E. (1979) *J. Biol. Chem. 254*, 259–261.

Marcus, F., & Harrsch, P. B. (1990) *Arch. Biochem. Biophys. 279*, 151–157.

Marcus, F., Edelstein, I., Reardon, I., & Heinrikson, R. L. (1982) *Proc. Natl. Acad. Sci. U.S.A. 79*, 7161–7165.

McGrane, M. M., El-Maghrabi, M. R., & Pilkis, S. J. (1983) *J. Biol. Chem. 258*, 10445–10454.

Meek, D. W., & Nimmo, H. G. (1983) *FEBS Lett. 160*, 105–109.

Nimmo, H. G., & Tipton, K. F. (1975) *Eur. J. Biochem. 58*, 575–585.

Pilkis, S. J., El-Maghrabi, M. R., Pilkis, J., & Claus, T. H. (1981) *J. Biol. Chem. 256*, 3619–3622.

Pilkis, S. J., Claus, T. H., Kountz, P. D., & El-Maghrabi, M. R. (1987) in *The Enzymes*, Vol. 18, 3rd ed., pp 3–46, Academic Press, New York.

Pontremoli, S., Grazi, E., & Accorsi, A. (1968) *Biochemistry 7*, 3628–3633.

Pontremoli, s., Melloni, E., Michetti, M., Salamino, F., Sparatore, B., & Horecker, B. L. (1982) *Arch. Biochem. Biophys. 218*, 609–613.

Raines, C. A., Lloyd, J. C., Longstaff, M., Bradley, D., & Dyer, T. (1988) *Nucleic Acids Res. 16*, 7931–7942.

Sarngadharan, M. G., Watanade, A., & Pogell, B. (1969) *Biochemistry 8*, 1411–1419.

Schirmer, T., & Evans, P. R. (1990) *Nature 343*, 140–145.

Tejwani, G. A. (1983) *Adv. Enzymol. Relat. Areas Mol. Biol. 54*, 121–194.

Tejwani, G. A., Pedrosa, F. O., Pontremoli, S., & Horecker, B. L. (1976) *Arch. Biochem. Biophys. 177*, 253–264.

Van Schaftingen, E. (1987) *Adv. Enzymol. Relat. Areas Mol. Biol. 59*, 315–395.

Van Schaftingen, E., & Hers, H. G. (1981) *Proc. Natl. Acad. Sci. U.S.A. 78*, 2861–2863.